

Cite this article as: Zhao Fengyuan, Ye Yicong, Zhang Zhouan, et al. Interpretable Machine Learning Model-Based Phase Prediction for Refractory High-Entropy Alloys[J]. Rare Metal Materials and Engineering, 2023, 52(04): 1192-1200.

ARTICLE

Interpretable Machine Learning Model-Based Phase Prediction for Refractory High-Entropy Alloys

Zhao Fengyuan, Ye Yicong, Zhang Zhouan, Li Yahao, Wang Jie, Tang Yu, Li Shun, Bai Shuxin

Department of Materials Science and Engineering, College of Aerospace Science and Engineering, National University of Defense Technology, Changsha 410073, China

Abstract: Five machine learning (ML) approaches, i.e. K-Nearest Neighbor (KNN), Support Vector Machine (SVM), Decision Tree (DT), Random Forest (RF) and Artificial Neural Network (ANN) were used to classify and to predict the combination of phases, i.e. solid solutions (SS) and mixed solid solution and intermetallic (SS+IM) in refractory high-entropy alloys (RHEAs). Five input characteristic phase predicting parameters and 139 RHEAs were selected to train these models. Results show that ANN model has the highest accuracy of 90.72%. Experimental results of 9 quaternary and $(\text{TiVTa})_x\text{Cr}_{1-x}$ RHEAs verify the accuracy of prediction and indicate that RF and ANN can predict more accurately, successfully predicting 11 SS and 3 SS+IM. SHAP (SHapley Additive exPlanations) model was used to interpret the ANN model which exhibits the highest accuracy and to investigate the contribution of each feature to phase formation. The order of importance of five features is enthalpy of mixing (ΔH_{mix}), atomic size difference (δ), valence electron concentration (VEC), entropy of mixing (ΔS_{mix}), and electronegativity difference ($\Delta\chi$), where the mean SHAP value of ΔH_{mix} is approximately 5 times higher than that of $\Delta\chi$ and 4 times higher than that of ΔS_{mix} . Less negative ΔH_{mix} , smaller δ and VEC may contribute to the formation of SS in RHEAs.

Key words: machine learning; refractory high-entropy alloys; model interpretability; solid solution; intermetallic

High entropy alloy (HEA) is a new concept of alloy design, first developed by Cantor^[1] and Yeh^[2] in 2004. By mixing equiatomic or near-equiatomic multi-element (≥ 4 , usually), HEAs show some potentials in overcoming the constraints of the inherent properties of one or two main elements in traditional alloys, and achieve “free” design in the atomic level^[3-4]. Among all kinds of HEAs, refractory high entropy alloys (RHEAs) usually consist of refractory elements: Cr, Hf, Mo, Nb, Ta, Ti, V, W, and Zr, sometimes with minor addition of Al, Ni, Si, C, O, etc^[5]. Some RHEAs exhibit a variety of excellent properties, such as high strength^[4-6], sufficient plasticity^[7-9], wear resistance^[10], radiation resistance^[11-12] and particularly high strength at elevated temperature^[13-15], which makes them applicable in a wider range of fields.

The formation of solid solutions (SS) instead of complex intermetallics (IM) is normally desired in RHEAs, because the

formation of IM such as Laves phase^[16] usually brings about brittleness, making RHEAs inappropriate as structural materials. Thus, the efficient and accurate prediction of phase formation in RHEAs composed of certain elements is of great significance in tailoring the properties and performance. Due to the vast combinations of elements and compositions, the traditional “trial and error” methods cannot meet the growing requirement for highly efficient development of new HEAs. Some empirical rules^[17-18] regarding the trends of phase formation have been established to guide the design of HEAs. High ΔS_{mix} is regarded as an important factor in promoting the formation of multi-principal solid solutions whereas large, negative values of ΔH_{mix} will destabilize SS phases by competing with ΔS_{mix} and thus be prone to IM phase formation^[16,19]. The electronegativity difference of $\Delta\chi$ is related to the elemental segregation and the formation of

Received date: September 20, 2022

Foundation item: National Natural Science Foundation of China (U20A20231, 11972372); College of Aerospace Science and Engineering Youth Talent Fund, National University of Defense Technology (KY0505072209)

Corresponding author: Zhang Zhouan, Ph. D., Lecturer, Department of Materials Science and Engineering, National University of Defense Technology, Changsha 410072, P. R. China, Tel: 0086-731-87007225, E-mail: zrzhang@nudt.edu.cn

Copyright © 2023, Northwest Institute for Nonferrous Metal Research. Published by Science Press. All rights reserved.

topologically close packed (TCP) phases^[19]. Atom size mismatch δ and the mixing enthalpy ΔH_{mix} are well-known empirical criteria for amorphous (AM) alloys^[16,19], which show potentials in separating SS and AM phases in HEAs. The valence electron concentration (VEC) has been used as a critical parameter in determining the formation of fcc or bcc phase^[19]. However, due to the variability of element composition and the complexity of alloy system, these empirical approaches seems insufficient for accurately predicting the phase types of HEAs^[17].

Compared with the empirical methods, other computer-aided calculation methods, such as phase diagram calculation (CALPHAD)^[20], molecular dynamics simulation^[21] and density functional theory calculation (DFT)^[22], have also been increasingly used to discover correlations between material structures and properties. There are successful cases in the prediction of the structure and electronic properties of HEAs^[20-21], but the accurate prediction is time-consuming and limited by computational capacity. Therefore, it is urgent to use new methods in order to achieve tailored HEAs with desired properties by establishing the relationship between composition and phase formation.

Machine learning (ML) is a broad class of data-driven algorithms used to make inferences and classifications from data. As a data-driven algorithm, ML is suitable for the study of high-dimensional problems, particularly prominent in HEAs design and has been successfully used in the prediction of phases in HEA systems^[23-24]. Various properties, including the composing elements, thermodynamic parameters, etc, have been considered as input features for the phase prediction and ML models with overall high accuracy (>75%) have been trained based on dataset containing usually a few hundred sub-entries. For example, Islam et al^[25] trained an ANN model to predict the formation of AM, SS and IM based on 118 HEAs with an average accuracy of more than 80%. Krishna et al^[26] used Logistic regression (LR), SVM, DT, RF, Gradient Boosting (GB) and ANN to predict SS or SS+IM based on 636 HEAs data, among which SVM showed the highest accuracy of 83.02%. Agarwal et al^[23] used adaptive neuro fuzzy interface system to predict the fcc and bcc phases in HEAs with elemental composition and thermodynamic parameters as input features, and the accuracy reached 84.21%. Similar works were conducted by Dai^[27] and Risal et al^[28]. Qi et al^[29] extracted more than 600 entries from binary alloy systems and the trained RF model showed the highest accuracy over 80%. However, the dataset used so far is heavily biased towards alloys mainly composed of 3d transitional metals, such as Cr, Mn, Fe, Co and Ni. The specific datasets of refractory HEAs and corresponding ML-based phase prediction are relatively rare. There are many differences between RHEAs and the 3d-transition HEAs in terms of composing elements, essential physical parameters, possible phases and correspondingly intrinsic properties. The models used for successful classification and prediction of phases in 3d-transition HEAs may not be applicable for RHEAs.

Therefore, in the present study, we attempted to fill the gap in the research and predicted the phase formation in RHEAs using five ML algorithms with supervised learning, namely K-Nearest Neighbor (KNN), Support Vector Machine (SVM), Decision Tree (DT), Random Forest (RF) and Artificial Neural Network (ANN) based on 139 datasets and verified the accuracy of models by examining 9 quaternary and (TiVTa)_xCr_{1-x} RHEAs. SHAP (SHapley Additive exPlanations) model^[30] was used to interpret the models and to shed light on the physical influence of different features on the phase formation, and the relative feature importance was obtained.

1 Materials and Methods

A schematic flow chart of the approach used for phase prediction of RHEAs based on ML is displayed in Fig. 1. Firstly, 139 RHEAs were selected from Ref.[31] which consist of 97 SS (there are only solid solution phases) and 42 SS+IM (there are both solid solution and intermetallic phases) for prediction and analysis. It is worth noting that alloys with a mixture of solid solution phases such as multiple bcc phases or bcc+hcp phases are considered as the SS category and alloys containing intermetallic phases such as Laves phase are considered as the SS+IM category. After screening the dataset, the major composing elements of 139 RHEAs are refractory metals, which are Ti, V, Cr, Zr, Nb, Mo, Hf and Ta. Some alloys also contain a minor percentage of non-refractory elements, such as Si, Al and C, which are usually added to tailor the properties of RHEAs.

Each data was labeled so that every data point had a target label, and the labeled dataset was then used to train the model. The input features include entropy of mixing (ΔS_{mix}), enthalpy of mixing (ΔH_{mix}), atomic size difference (δ), electronegativity difference ($\Delta\chi$), and valence electron concentration (VEC) with definitions in Table 1. Some representative subsets are displayed in Table 2.

Five ML algorithms which are KNN, SVM, DT, RF and

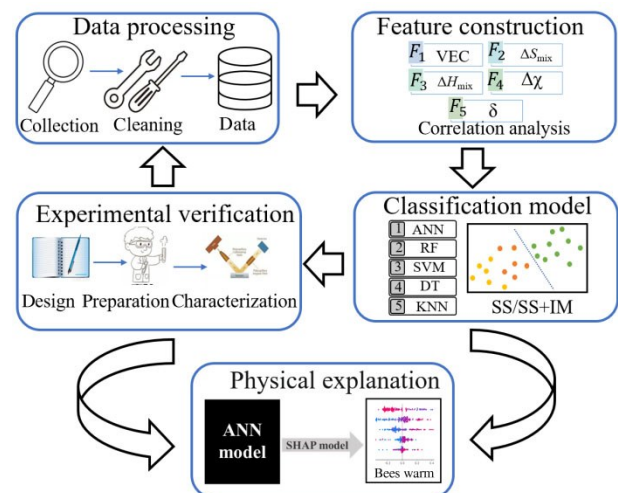


Fig.1 Schematic flow chart of phase prediction for RHEAs based on ML method

Table 1 Description of the parameters used in this study

Feature	Equation
Valence electron concentration, VEC	$VEC = \sum_{i=1}^n c_i VEC_i$
Difference of the pauling, negativities, $\Delta\chi$	$\Delta\chi = \sqrt{\sum_{i=1}^n c_i (\chi_i - \bar{\chi})^2}$
Atomic size difference, δ	$\delta = 100 \times \sqrt{\sum_{i=1}^n c_i \left(1 - \frac{r_i}{\bar{r}}\right)^2}$
Mixing enthalpy, ΔH_{mix}	$\Delta H_{mix} = \sum_{i=1, i < j}^n 4H_{ij} c_i c_j$
Mixing entropy, ΔS_{mix}	$\Delta S_{mix} = -R \sum_{i=1}^n c_i \ln c_i$

Table 2 Some representative subsets in the dataset

RHEAs	ΔS_{mix}	$\Delta\chi$	VEC	δ	ΔH_{mix}	Classification
MoNbTaW	11.53	0.36	5.50	2.17	-4.75	SS
Al _{0.75} MoNbTiV	13.33	0.23	4.68	3.86	-11.12	SS
HfMo _{0.5} NbTiV _{0.5}	12.97	0.25	4.63	5.94	-0.88	SS
CrMo _{0.5} NbTa _{0.5} TiZr	13.37	0.31	4.08	20.27	-4.92	SS+IM
Co ₂ Cr _{0.5} Ni ₂ VW _{0.5}	12.02	0.18	8.17	3.19	-8.92	SS+IM
Mo ₂ NbTiVZr	12.98	0.31	5.00	6.58	-3.67	SS+IM

accuracy of five ML algorithms is defined as the number of times by which ML approaches can correctly identify a target, which is type of RHEAs phases (SS or SS+IM) in this project. It is worth noting that the accuracy is obtained based on the average accuracy. These models based on the experience data gained through training were then used for examination of the formed phase in 9 quaternary and (TiVTa)_xCr_{1-x} RHEAs. Lastly, SHAP model^[30] was used to investigate the roles of different features in classifying SS and SS+IM and the relative importance of these features was obtained.

The predictive capability of our approach was verified by experimental study on 9 quaternary and (TiVTa)_xCr_{1-x} RHEAs, which were prepared by arc-melting and suction-casting. High-purity raw metals (>99.95%) were melted in the vacuum furnace under a Ti-gettered argon atmosphere. The ingot was remelted at least six times to achieve a homogeneous distribution of elements and then suction-casted to obtain a 10 mm×10 mm×70 mm ingot. The specimens with the dimension

of 2 mm×10 mm×10 mm were firstly ground and polished to achieve a flat surface, and then characterized by X-ray diffractometer (XRD, Rigaku SmartLab 9 kW).

ANN were used. Statistical analysis was carried out using the Matlab2018b software and the scikit-learn library^[32]. Data imported into the Matlab2018b consisted of six attributes which include five features as displayed above and one output corresponding to the phase composition. Details of the application of the supervised learning approach can be found in Ref.[33].

In order to avoid overfitting of the models, the cross-validation method^[25] was used and the dataset was randomly divided into 4 subsets containing 35, 35, 35 and 34 cases. Fig.2 displays the setup of the cross-validation method. The

of 2 mm×10 mm×10 mm were firstly ground and polished to achieve a flat surface, and then characterized by X-ray diffractometer (XRD, Rigaku SmartLab 9 kW).

2 Results and Discussion

2.1 Model construction and phase prediction

The data dependence of each design parameter is shown in the scatter plot (Fig. 3) with histograms of all parameters considered in the diagonal. The overlapping of the graph indicates that the identification of phases using a single empirical parameter is explicitly insufficient and thus all parameters need to be considered for ML algorithms due to the multi-dimensional features in alloy design. The interdependence of each parameter for phase prediction is shown by plotting the heatmap with the Pearson correlation coefficient^[25] in Fig.4. It is well established that the value of 1 suggests a strong positive correlation whereas -1 suggests a strong negative correlation between the parameters. As shown in Fig.4, the correlation value varies between -0.36 and 0.32, which suggests that there are no strong correlations between each pair of features.

In the DT classifier, Gini impurity was used as the criteria^[34] for finding the leaf node. When the maximum depth (starting from the root node to the leaf node) is 7, the highest accuracy achieved is 85.63%.

In the RF classifier, the value of n estimators corresponding to the number of trees in the forest^[26] varies from 10 to 100 with an interval of 10 and the maximum depth varies from 1 to 10. The highest accuracy obtained is 88.57% with the number of trees as 10 and the maximum depth (the number of branches) as 5.

In the KNN classifier, the Euclidean distance algorithm^[35]

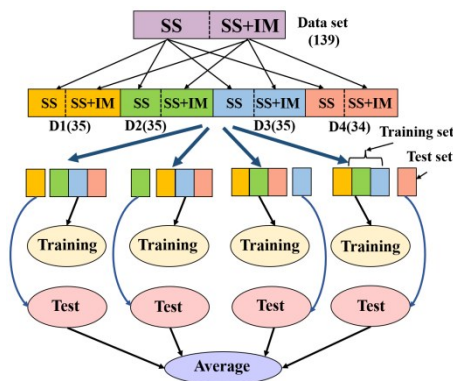


Fig.2 Illustration of the 4-fold cross-validation method

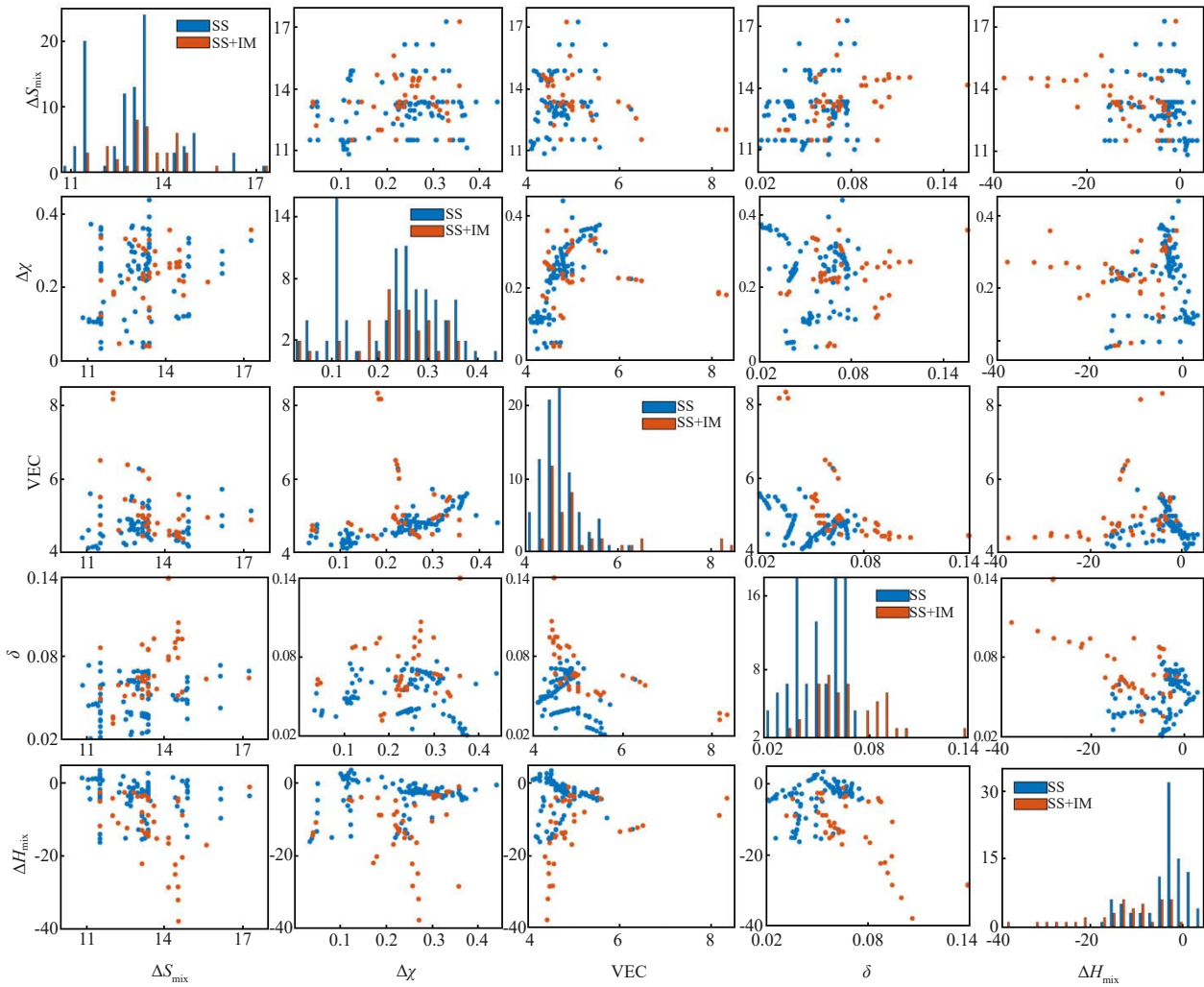


Fig.3 Scatter plots and histograms of design parameters used for RHEAs prediction

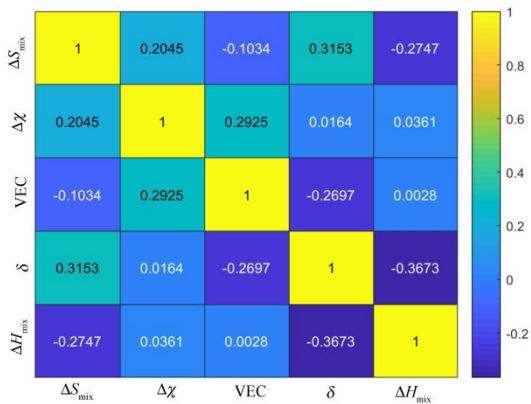


Fig.4 Heatmap of alloys with SS+IM phases showing no strong correlation between each pair of features

was selected to compute the distance between the testing data

and training data. With a pre-set k value, k -nearest training samples were first selected, and the dominant label among these training data was assigned to the testing data. We adjusted the value of k from 1 to 10. The accuracy for different k values in details are listed in Table 3 and the highest accuracy obtained is 84.94% when $k=3$.

In the SVM classifier, Radial basis function kernel was used for the non-linearly separable data^[26]. The value of the regularization parameter varies from 0.01 to 16, and the value of the kernel coefficient (γ) varies from 0.0001 to 2. The highest accuracy is 86.34% when the regularization parameter is 13 and $\gamma=2$. It is worth mentioning that the best combination of parameters in the RF classifier and SVM classifier are obtained using gridsearchcv function^[32].

In the ANN classifier, the number of the hidden layers changes from 1 to 3 and the number of the neurons in each layer changes from 3 to 6. A rectified linear unit (ReLU)

Table 3 Accuracy of KNN under different k values

k value	1	2	3	4	5	6	7	8	9	10
Accuracy/%	84.16	82.73	84.94	79.14	82.02	80.57	79.87	79.85	79.87	78.85

activation function was used in the hidden layer^[25], and the softmax activation function was used in the output layer. The loss was analyzed using the binary cross-entropy method^[25], and the learning rate was set at 0.001. Fig. 5 shows the relationship between the loss and accuracy of ANN models. As shown in Fig. 5, the smallest loss and the highest accuracy are achieved when the number of hidden layers is 2 and the number of neurons is 5 (2×5), which is marked by the pink diamond. Table 4 shows the loss and accuracy in details using a certain number of hidden layers and neurons in each layer. The minimum loss and the highest accuracy are 0.13 and 90.72%, respectively when using 2 hidden layers and 5 neurons in each hidden layer, which are used throughout the follow-up discussion.

Table 5 displays the accuracy of five different ML algorithms used in the present study, relevant published results based on different datasets and the ML model showing the highest accuracy in each study. All five ML algorithms in the present study yield high accuracy ($\geq 85\%$) and the highest accuracy is 90.72% using the ANN model. Compared with the published results^[26,28,35] which aim at classifying between SS and SS+IM, ANN and SVM models in the present study outperform those models. Although there are only 139 subentries in the present dataset, slightly smaller compared

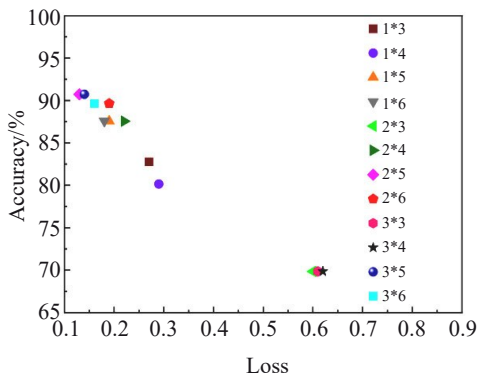


Fig. 5 Relationship between loss and accuracy of ANN model

Table 4 Average loss and accuracy of ANN method

Number of hidden layers	Number of neurons	Loss	Accuracy/%
1	3	0.27	82.76
1	4	0.29	80.15
1	5	0.19	87.56
1	6	0.18	87.56
2	3	0.61	69.85
2	4	0.22	87.56
2	5	0.13	90.72
2	6	0.19	89.63
3	3	0.61	69.85
3	4	0.62	69.85
3	5	0.14	90.72
3	6	0.16	89.63

Table 5 Comparison of model accuracy

Ref.	Alloys	Dataset	Best accuracy/%	Outputs
[25]	HEAs	118	>80 (ANN)	AM/SS/IM
[26]	HEAs	636	83.03 (SVM)	SS/SS+IM
[27]	HEAs	407	91 (LR)	FCC/BCC/HCPAM
[28]	HEAs	598	85.91 (ANN)	SS/IM/SS+IM
[29]	HEAs	614	>80 (RF)	fcc/bcc/hcp/fcc+bcc
[35]	HEAs	347	78.9 (ANN)	SS/SS+IM
This work	RHEAs	139	90.72 (ANN)	SS/SS+IM
This work	RHEAs	139	86.34 (SVM)	SS/SS+IM
This work	RHEAs	139	88.57 (RF)	SS/SS+IM
This work	RHEAs	139	85.63 (DT)	SS/SS+IM
This work	RHEAs	139	84.94 (KNN)	SS/SS+IM

with other studies, all models still reach overall high accuracies, especially ANN and SVM. The possible reasons behind this outperformance are higher quality of sub-entries (more oriented towards RHEAs) and better selection of hyperparameters used in the training.

The performance of five ML algorithms in terms of identifying SS and SS+IM was further analyzed using the confusion matrix^[26]. Fig. 6 shows the confusion matrix with normalized values for actual and predicted phases using five algorithms regarding the classification of SS+IM and SS. The diagonal (dark blue) shows the true positive and negative, which implies that the classification is correct. ANN shows the highest accuracy overall in predicting both SS+IM and SS, reaching 89.7% and 90.9%, respectively. The second best is RF. It is possible that under the combined action of multiple trees, the RF algorithm reduces the error caused by a single decision tree to a certain extent, thereby improving the accuracy of the DT model. Apart from ANN and RF, other three models show higher accuracy in predicting the SS category with the ranking of accuracy as SVM>DT>KNN. However, the accuracy for the prediction of SS+IM is lower than 0.78 which is possibly due to the imbalanced dataset where there are 97 subsets for SS and only 42 subsets for SS+IM. The more frequently types of datasets the training model learns, the more dominant the type of datasets during prediction.

Table 6 shows a summary of ML algorithms and the corresponding accuracies in previous HEA phase prediction and the present study. Like this work, most research simultaneously used several ML algorithms for phase prediction. In general, ANN has relatively high accuracy (the highest is in Ref.[28, 35] and the present study) in HEA phase prediction, which is possibly because ANN perform better in handling unbalanced dataset like the current case^[35]. The performance of other ML algorithms is related to the quality and size of the training dataset, the input features, the selection of hyperparameters and the methods used to avoid overfitting^[26-28]. All five models in the present study show high accuracy ($\geq 85\%$) due to the specialized RHEA dataset with high fidelity and a careful selection of hyperparameters.

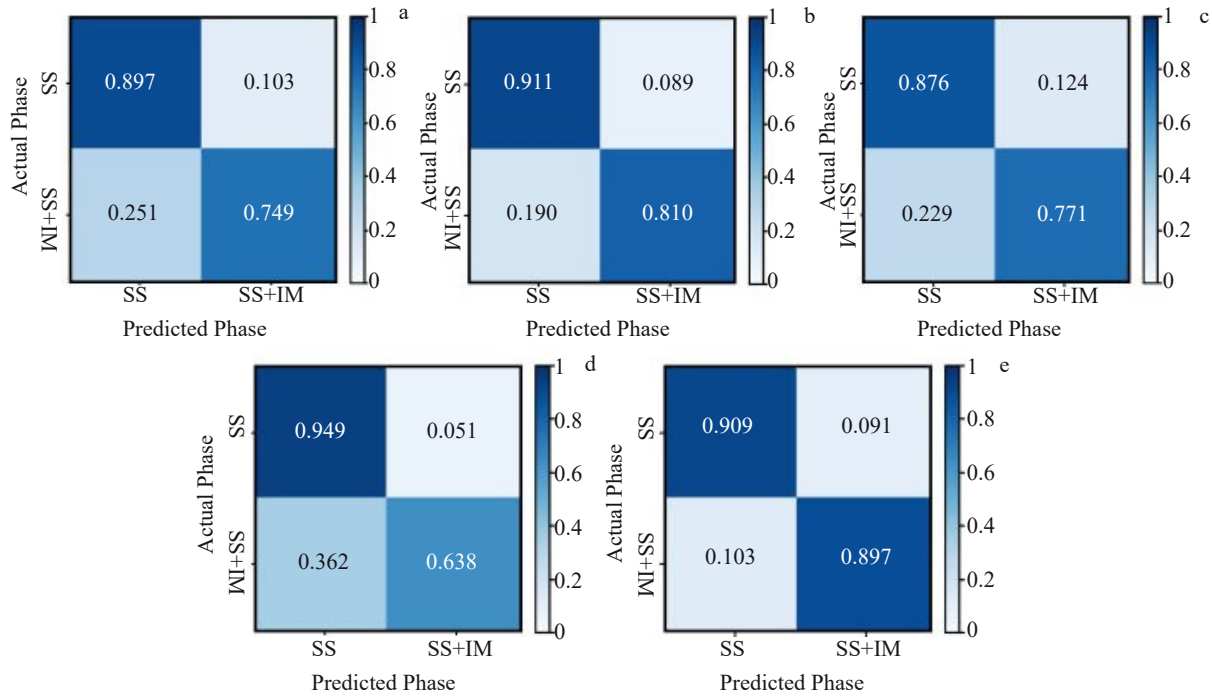


Fig.6 Confusion matrix of DT (a), RF (b), KNN (c), SVM (d) and ANN (e)

Table 6 Accuracy of ML algorithms used in previous study and this work (%)

Ref.	ANN	SVM	DT	RF	KNN	LR	GB
[25]	80	-	-	-	-	-	-
[26]	80.5	83.02	77.99	82.39	-	62.89	81.3
[27]	-	59.5	78	80	-	91	82.5
[28]	85.91	84.4	-	83.7	83.98	-	-
[29]	-	-	-	80	-	-	-
[35]	78.9	73.2	-	-	-	-	-
This work	90.72	86.34	85.63	88.57	84.94	-	-

2.2 Experimental validation

To test the applicability of our model, we prepared 9 new quaternary RHEAs that are not contained in the dataset. Fig. 7 shows the XRD patterns of the as-cast 9 quaternary RHEAs. VCrNbMo, TiVCrMo, TiVCrNb, VNbHfTa and TiVZrHf alloys exhibit only one set of peaks corresponding to bcc. There are two sets of peaks for VZrNbTa and ZrNbMoTa alloys which are indexed as two bcc phases, but still in the SS category. In contrast, the composing phases are complex including at least one SS phase and one Laves phase in CrZrNbMo and TiVCrZr alloys, and thus they are classified as the SS+IM category. Furthermore, due to the possible formation of intermetallic phases according to the Ti-Cr and Ta-Cr binary phase diagrams, we also prepared a series of $(\text{TiVTa})_x\text{Cr}_{1-x}$ alloys in order to investigate the effect of content of Cr on the formation of phases. Fig. 8 shows the XRD patterns of $\text{Ti}_{32}\text{V}_{32}\text{Ta}_{31}\text{Cr}_5$, $\text{Ti}_{30}\text{V}_{30}\text{Ta}_{30}\text{Cr}_{10}$, $\text{Ti}_{28}\text{V}_{28}\text{Ta}_{29}\text{Cr}_{15}$, $\text{Ti}_{27}\text{V}_{27}\text{Ta}_{26}\text{Cr}_{20}$ and TiVTaCr alloys. There are only one set of peaks indexed as bcc except for TiVTaCr which also shows another set of peaks indexed as a Laves phase.

Five trained models were used to predict the phases of 9 quaternary and $(\text{TiVTa})_x\text{Cr}_{1-x}$ RHEAs. The predicted results, actual phases and corresponding categories are shown in Table 7. With regards to the quaternary alloys, all five models predict the SS category correctly but only SVM, RF and ANN models correctly predict the SS+IM category (CrZrNbMo and TiVCrZr). In terms of the $(\text{TiVTa})_x\text{Cr}_{1-x}$ alloys, only RF and ANN models predict the phases of all five alloys correctly. RF and ANN exhibit higher accuracy, successfully predicting 11 SS and 3 SS+IM. KNN and SVM models fail to grasp the formation of IM in TiVCrTa and DT overall performs the worst among the five models. Therefore, one can conclude that the results predicted by RF and ANN models agree well with the experimental results.

The results again suggest better accuracy in predicting SS category, in agreement with the predictive capability shown in Fig. 6. RF and ANN show higher accuracy in predicting alloys belonging to SS+IM category (0.81 and 0.897, respectively), agree well with experimental validation. As mentioned above, the whole dataset is imbalanced where there are 97 SS subsets

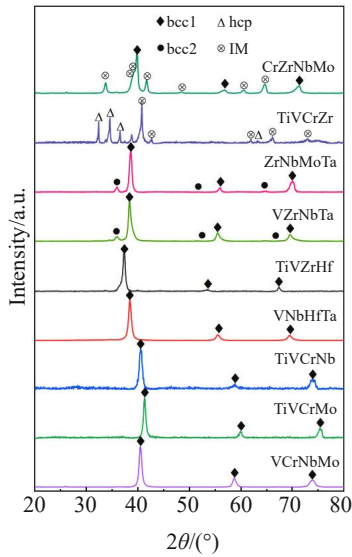
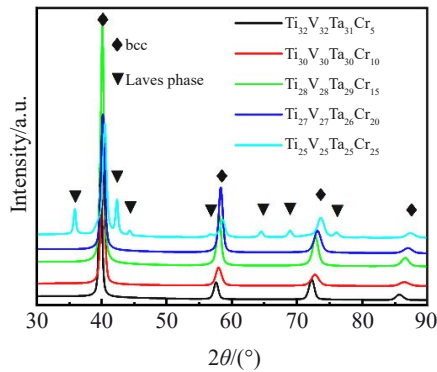


Fig.7 XRD patterns of 9 new RHEAs outside of the dataset

Fig.8 XRD patterns of $(\text{TiVTa})_x\text{Cr}_{1-x}$ alloys

and only 42 SS+IM subsets. Furthermore, the majority of alloys in the dataset belonging to the SS+IM category contain one or two minor elements, such as Si, Co, Al and C, which

inevitably affect the trained models through learning from δ , VEC, ΔH_{mix} , ΔS_{mix} and $\Delta\chi$. For instance, the addition of Si, leading to a drastic increase in δ , may overstress the importance of δ in classifying SS and SS+IM. Thus, when RHEAs are only composed of refractory elements, like the 9 cases in the current study, the trained models may be unable to effectively pick up the differences of five input features and inaccurately categorize the original SS+IM as SS. Overall, SVM, RF and ANN show good generalization ability in predicting both SS and SS+IM, which may contribute to understanding and discovery of advanced RHEAs.

2.3 Feature importance analysis

Since ANN shows the highest accuracy in prediction, the relative importance of each feature was investigated using SHAP model based on the ANN model.

The average Shapley values (SHAP value) [30] of five features are displayed in Fig.9a with a bees-warm diagram in Fig.9b. Each point in Fig.9b is the value of a subset in the dataset. According to the color bar of Fig.9b, the darker the red, the larger the value, and the darker the blue, the smaller the value. The abscissa indicates the SHAP value of each subset with the value 1 as IM and the value 0 as SS, which means that the closer the value to 1, the easier the formation of IM. The more positive the value, the higher the tendency to form IM, whereas the more negative the value (larger absolute value), the higher the tendency to form SS.

As shown in Fig.9a, the order of importance of five features is ΔH_{mix} , δ , VEC, ΔS_{mix} and $\Delta\chi$. The mean SHAP value of ΔH_{mix} is approximately 5 times higher than that of $\Delta\chi$ and 4 times higher than that of ΔS_{mix} , showing the most important role of ΔH_{mix} in distinguishing SS and SS+IM in this dataset. As shown in Fig.9b, the larger the ΔH_{mix} (smaller absolute value), the easier it is to form SS, and the smaller the ΔH_{mix} , the easier it is to form IM. The atomic size mismatch (δ) and valence electron concentration (VEC) are the second and third important factor affecting the phase formation, and the smaller

Table 7 Predicted results of 9 RHEAs using five different algorithms and their actual phases characterized by XRD

Alloys	KNN	SVM	DT	RF	ANN	XRD	Category
VCrNbMo	SS	SS	SS	SS	SS	bcc	SS
CrZrNbMo	SS	SS+IM	SS	SS+IM	SS+IM	bcc+IM	SS+IM
TiVCrMo	SS	SS	SS	SS	SS	bcc	SS
TiVCrNb	SS	SS	SS	SS	SS	bcc	SS
TiVCrZr	SS	SS+IM	SS	SS+IM	SS+IM	hcp +IM+unknown	SS+IM
VNbHfTa	SS	SS	SS	SS	SS	bcc	SS
TiVZrHf	SS	SS	SS	SS	SS	bcc	SS
ZrNbMoTa	SS	SS	SS	SS	SS	bcc1+bcc2	SS
VZrNbTa	SS	SS	SS	SS	SS	bcc1+bcc2	SS
$\text{Ti}_{32}\text{V}_{32}\text{Ta}_{31}\text{Cr}_5$	SS	SS	SS	SS	SS	bcc	SS
$\text{Ti}_{30}\text{V}_{30}\text{Ta}_{30}\text{Cr}_{10}$	SS	SS	SS	SS	SS	bcc	SS
$\text{Ti}_{28}\text{V}_{28}\text{Ta}_{29}\text{Cr}_{15}$	SS	SS	SS+IM	SS	SS	bcc	SS
$\text{Ti}_{27}\text{V}_{27}\text{Ta}_{26}\text{Cr}_{20}$	SS	SS	SS+IM	SS	SS	bcc	SS
$\text{Ti}_{25}\text{V}_{25}\text{Ta}_{25}\text{Cr}_{25}$	SS	SS	SS+IM	SS+IM	SS+IM	bcc+Laves	SS+IM

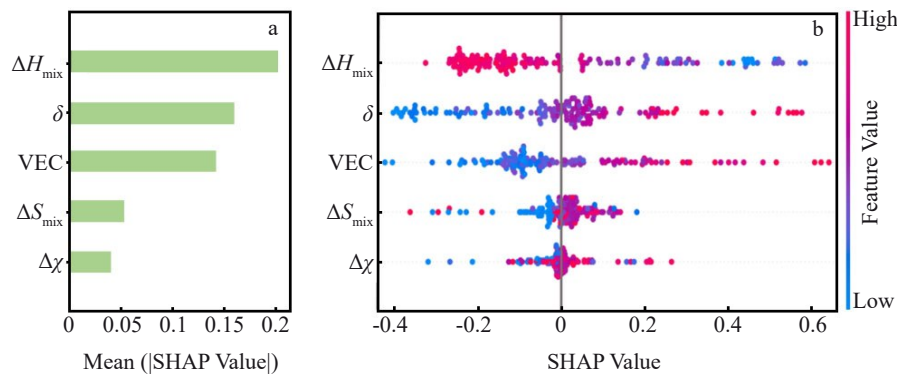


Fig.9 Average SHAP value of five features (a) and bees warm diagram of SHAP value (b) based on the ANN model

the value of them, the easier it is to form SS, which is in agreement with the Hume-Rothery law that has long emphasized the importance of VEC and δ in traditional solid-solution alloys.

The majority of the SHAP values for ΔS_{mix} and $\Delta\chi$ are concentrated around 0, indicating the least influence on phase formation among these five features. Li et al^[36] showed that $\Delta\chi$ has no direct effect on the formation of phases in eutectic HEAs. Yang et al^[17] claimed that the mixing entropy does not determine the formation of solid solutions in HEAs. However, what is worth noting is that the calculation of ΔS_{mix} in the dataset is based on the assumption that all alloys are ideal solid solutions, which may not grasp the true mixed entropy in the RHEAs with complex crystal structures and multiple sublattices. New metrics describing the entropy of these RHEAs are needed in order to assess the contribution of entropy in terms of phase formation, and related work is in progress.

3 Conclusions

1) Five ML approaches (KNN, SVM, DT, RF and ANN) are used to classify and to predict the combination of phases, i.e., solid solution (SS) and mixed solid solution and intermetallic (SS+IM) in RHEAs. Five input features, including the atomic size difference δ , the mixing entropy ΔS_{mix} , the mixing enthalpy ΔH_{mix} , the valence electron concentration VEC and the electronegativity difference $\Delta\chi$, and 139 RHEAs from the literature are selected to train these models. ANN shows the highest accuracy of 90.72% whereas other four models show higher accuracy in predicting SS (>87%) but relatively low accuracy in predicting SS+IM (<81%), possibly due to the imbalanced dataset.

2) Nine quaternary and (TiVTa)_xCr_{1-x} RHEAs are prepared and characterized by XRD, which experimentally validates the applicability of the trained models. RF and ANN exhibit higher accuracy, successfully predicting 11 SS and 3 SS+IM whereas SVN, DT and KNN can only accurately predict the SS category. SHAP model can characterize the roles of different features on the phase formation, in which ΔH_{mix} , δ and VEC are more important in determining the phase formation whereas the impact of ΔS_{mix} and $\Delta\chi$ is the minimal.

The formation of solid solution is more likely if the RHEA shows less negative value of ΔH_{mix} and smaller δ and VEC.

3) Overall, this study provides an efficient ML approach in phase prediction of RHEAs and elucidates the specific influence of five different features on phase formation, which shows some potential in the acceleration of future RHEA design.

References

- 1 Cantor B, Chang I, Knight P et al. *Materials Science and Engineering A*[J], 2004, 375–377: 213
- 2 Yeh J W, Chen S K, Lin S J et al. *Advanced Engineering Materials*[J], 2004, 6(5): 299
- 3 Senkov O N, Miracle D B. *Acta Materialia*[J], 2017, 122: 448
- 4 Lei Z F, Liu X J, Wu Y et al. *Nature*[J], 2018, 563(7732): 546
- 5 Senkov O N, Miracle D B, Chaput K J et al. *Journal of Materials Research*[J], 2018, 33(19): 3092
- 6 Rw A, Yu T A, Zlb C et al. *Materials & Design*[J], 2021, 213: 110 356
- 7 Wei S L, Kim S J, Kang J et al. *Nature Materials*[J], 2020, 19(11): 1175
- 8 An Z B, Mao S C, Yang Tao et al. *Materials Horizons*[J], 2021, 8(3): 948
- 9 Zhang Z R, Tang Y. *Materials & Design*[J], 2017, 133: 435
- 10 Luo J, Sun W, Duan R et al. *Science & Technology*[J], 2022, 110: 43
- 11 Atwani O El, Li N, Li M et al. *Science Advances*[J], 2019, 5(3): 2002
- 12 Zhang Z, Armstrong D, Grant P S. *Progress in Materials Science*[J], 2021, 123: 100 807
- 13 Chen S Y, Tong Y, Tseng K K et al. *Scripta Materialia*[J], 2019, 158: 50
- 14 Andreoli A F, Mendes R G, Witusiewicz V T et al. *Acta Materialia*[J], 2021, 221: 117 416
- 15 Senkov O N, Jensen J K, Pilchak A L et al. *Materials & Design*[J], 2018, 139: 498
- 16 Miracle D B, Senkov O N. *Acta Materialia*[J], 2017, 122: 448
- 17 Yang X, Zhang Y. *Materials Chemistry and Physics*[J], 2012,

- 132(2–3): 233
- 18 Wang J, Tang Y, Li S et al. *Intermetallics*[J], 2022, 142: 107 436
- 19 Guo S. *Materials Science and Technology*[J], 2015, 31(10): 1223
- 20 Zeng Y, Man M, Bai K et al. *Materials & Design*[J], 2021, 202(8): 109 532
- 21 Ju S P, Lee I J, Chen H Y. *Journal of Alloys and Compounds*[J], 2021, 858: 157 681
- 22 Rabin D, Meshulam A, Fuks D et al. *Journal of Alloys and Compounds*[J], 2021, 874: 159 940
- 23 Agarwal A, Rao A K P. *JOM*[J], 2019, 71(10): 3424
- 24 Zhou Z, Zhou Y, He Q et al. *npj Computational Materials*[J], 2019, 5: 128
- 25 Islam N, Huang Zhuang W, H L. *Computational Materials Science*[J], 2018, 150: 230
- 26 Krishna Y V, Jaiswal U K, Rahul M R. *Scripta Materialia*[J], 2021, 197: 113 804
- 27 Dai D, Xu T, Wei X et al. *Computational Materials Science*[J], 2020, 175: 109 618
- 28 Risal S, Zhu W, Guillen P et al. *Computational Materials Science*[J], 2021, 192: 110 389
- 29 Qi J, Cheung A M, Poon S J. *Scientific Reports*[J], 2019, 9: 15 001
- 30 Lundberg S, Lee S I. *Conference and Workshop on Neural Information Processing Systems*[C]. California: MIT Press, 2017: 4768
- 31 Senkov O N, Miracle D B, Chaput K J et al. *Journal of Materials Research*[J], 2018, 33(19): 3092
- 32 Pedregosa F, Varoquaux G, Gramfort A et al. *Journal of Machine Learning Research*[J], 2011, 12: 2825
- 33 Takahashi K, Takahashi L. *Journal of Physical Chemistry Letters*[J], 2019, 10(2): 283
- 34 Cutler D R, Edwards T C, Beard K H et al. *Ecology*[J], 2007, 88(11): 2783
- 35 Huang W, Martin P, Zhuang H L. *Acta Materialia*[J], 2019, 169: 225
- 36 Li Y, Tang Y, Ye Y et al. *Rare Metal Materials and Engineering*[J], 2021, 50(5): 1635

基于可解释机器学习模型的难熔高熵合金相预测

赵凤媛, 叶益聪, 张周然, 李亚豪, 王 洁, 唐 宇, 李 顺, 白书欣

(国防科技大学 空天科学学院 材料科学与工程系, 湖南 长沙 410073)

摘要: 采用k近邻 (KNN)、支持向量机 (SVM)、决策树 (DT)、随机森林 (RF) 和人工神经网络 (ANN) 5种机器学习 (ML) 方法对RHEAs中固溶体 (SS)、混合固溶体和金属间化合物 (SS+IM) 进行了分类和预测。选择了5个输入相预测参数作为特征以及139组RHEAs数据以训练ML模型。结果表明, ANN模型的预测准确率最高, 达到90.72%。9组新的四元和(TiVTa)_xCr_{1-x}体系RHEAs的实验结果显示, RF和ANN的预测精度更高, 精准预测了11个SS和3个SS+IM合金的相组成。采用了SHAP (SHapley Additive exPlanations) 模型来解释精度最高的ANN模型, 并研究每个特征对相形成的贡献。5个特征的重要性顺序是混合焓 (ΔH_{mix})、原子尺寸差 (δ)、价电子浓度 (VEC)、混合熵 (ΔS_{mix}) 和电负性差 ($\Delta\chi$), 其中 ΔH_{mix} 的平均SHAP值大约是 $\Delta\chi$ 的5倍, 是 ΔS_{mix} 的4倍。较大的 ΔH_{mix} 、较小的 δ 和VEC可能有助于RHEA中固溶体的形成。

关键词: 机器学习; 难熔高熵合金; 模型可解释性; 固溶体; 金属间化合物

作者简介: 赵凤媛, 女, 1994年生, 博士生, 国防科技大学空天科学学院材料科学与工程系, 湖南 长沙 410073, E-mail: 1552996426@qq.com